

Dirac combs induced by a composite corrugation and its effects in transmission probability

Wei-Ran Cao¹, Yong-Long Wang^{1,2,*}, Xiao-Lei Chen³, Hua Jiang¹, Chang-Tan Xu¹, and Hong-Shi Zong^{2,4,5†}

¹ *School of Physics and Electronic Engineering, Linyi University, Linyi 276005, P. R. China*

² *Department of Physics, Nanjing University, Nanjing 210093, P. R. China*

³ *Linyi Radio Frequency and Station Management, Linyi 276000, P. R. China*

⁴ *Joint Center for Particle, Nuclear Physics and Cosmology, Nanjing 210093, P. R. China and*

⁵ *State Key Laboratory of Theoretical Physics, Institute of Theoretical Physics, CAS, Beijing 100190, P. R. China*

For an electron confined to a surface reconstructed by a dual-frequency corrugation, we deduce the effective Hamiltonian by the formula of geometric influences, obtain an additive scalar potential induced by curvature that consists of attractive wells, like Dirac combs, with many grades. The number of grade is closely related to the multiple frequency number of the high frequency of the composite corrugation. Subsequently, we calculate the transmission probability of confined electron by using the transfer matrix method, and find the resonant tunneling peaks becoming sharper and the transmission gaps substantially widening with increasing the multiple frequency number. As a potential application, the dual-frequency corrugation can be employed to select electrons with particular incident energy, as an electronic switch.

PACS Numbers: 73.50.-h, 73.20.-r, 03.65.-w, 02.40.-k

I. INTRODUCTION

With the rapid development of nanotechnology, the fabrication of electronic nanodevices with particular geometries is becoming easy, and therefore various two-dimensional (2D) nanosystems with corrugation are designed and implemented, such as corrugated films¹⁻⁵, bent and corrugated nanotubes⁶⁻¹⁰ and so on. Those successes in manufacture found the basis of investigating the curvature-tunable filter⁵. Those surfaces with corrugation are an important type of 2D systems with relative complex geometries. For an electron confined to a geometrically corrugated surface, the effective Hamiltonian does not only depend on the 2D intrinsic geometry, but also on the way that the geometrically deformed surface is embedded in three-dimensional (3D) Euclidean space¹¹. To deduce the effective Schrödinger equation, the thin-layer quantization formalism^{12,13} is a suitable approach. And the corresponding effective Hamiltonian can be easily calculated by the formula of geometric influences¹⁴ in the spirit of the thin-layer quantization scheme. For the thin-layer quantization approach, two experimental evidences are given by that the geometric potential has been realized in photonic topological crystals¹⁵, and the geometric momentum^{14,16,17} has been observed to govern the propagation of surface plasmon polaritons on metallic wires¹⁸. Now the geometric potential and the geometric momentum are two most important contributions of the thin-layer quantization scheme.

With the development of the thin-layer quantization theory^{12,13,19,20}, quantum electronic nanodevices are rapidly developing toward smaller size and more complex structures and geometries. When the size of electronic devices is small enough to be compared with de Broglie wavelength of confined electron, the quantum geometric effects will become very significant and can not be ig-

nored⁵. For a 2D curved surface system embedded in 3D Euclidean space¹⁴, the geometric effects are entirely determined by the geometric curvature. The curvature is greater, the associated radius is smaller, while the geometric effects become more significant. In order to investigate the effects of geometric potential manifestly, nanoscale corrugation was introduced into a thin film to investigate the affected electronic properties¹. They found that corrugation can generate a geometric potential to enhance electron scattering contribution to the stepwise resistivity. Recently, in our work we found that transmission gaps and resonant tunneling domains emerged from corrugation⁵. To the best of our knowledge, most of the investigations have been done on single frequency corrugation, and rarely involve dual-frequency or multiple-frequency corrugations. However, the dual-frequency corrugation was applicably used to describe 2D superlattice potential²¹. As a consequence, the geometric effects of dual-frequency corrugation need a further investigation.

In the present paper, we will consider a model including a dual-frequency corrugation, and focus on the influences of the multiple frequency number on the geometric potential, and on the transmission probability. The dual-frequency corrugation can contribute a list of attractive wells, like Dirac combs, with many grades. When the multiple frequency number is a larger positive integer, for the transmission probability, the resonant tunneling peaks become sharper, and the transmission gaps become wider. As a potential application, the results are useful for designing quantum-electromechanical circuits²²⁻²⁴ and thin film transistors²⁵.

This paper is organized as follows. In Sec. II, using the formula of geometric influences^{14,26,27}, we deduce the effective Hamiltonian for electron confined to a thin film reconstructed by dual-frequency corrugation, give the effective quantum equation, and discuss the properties of

the geometric potential. In Sec. III, we investigate the effects of the dual-frequency corrugation on transmission probability, especially the multiple frequency number of the high frequency composition. Finally in Sec. IV the conclusions are given.

II. QUANTUM DYNAMICS OF A PARTICLE CONFINED ON A PERIODICALLY CORRUGATED SURFACE

In quantum mechanics, a free microscopic particle can be described by a time-independent Schrödinger equation, that is

$$-\frac{\hbar^2}{2m^*}\nabla^2\psi = E\psi, \quad (1)$$

where \hbar is the Plank constant divided by 2π , m^* is the effective mass of particle, ∇^2 is the Laplace operator usually defined in a 3D flat spatial space, ψ is the wave function describing the motion of particle and E is the energy with respect to the wave function ψ .

When the free particle is confined to a curved surface, the effective dynamics would be changed by the geometry of the curved surface^{13,14}. In the spirit of the thin-layer quantization scheme, to investigate the effective quantum dynamics for a particle confined to a curved surface, the Schrödinger equation Eq. (1) should be originally defined in a 3D curvilinear coordinate system as below

$$-\frac{\hbar^2}{2m^*}\frac{1}{\sqrt{G}}\partial_i G^{ij}\sqrt{G}\partial_j\psi = E\psi, \quad (2)$$

where G and G^{ij} are the determinant and inverse of the metric tensor G_{ij} defined in a 3D curvilinear coordinate system, respectively, wherein $i, j = 1, 2, 3$ denote the three curvilinear coordinate variables. It is easy to check that the Laplace operator depends on the metric of 3D curvilinear coordinate system. Particularly, this metric does depend on q_3 , which leads to that the partial component in q_3 direction of the Laplace operator contributes a scalar potential in the effective Hamiltonian. Here q_3 stands for the coordinate variable normal to a curved surface.

A surface reconstructed by a dual-frequency corrugation \mathcal{S} (see Fig.1) that can be parametrized by

$$z = a \cos(n\gamma x) \sin(\gamma x), \quad (3)$$

where a denotes the amplitude of composite corrugation, $2\pi/\gamma$ describes the period length of corrugation, n is a nonzero positive integer which is named as a multiple frequency number because that it describes the high frequency composition of the dual-frequency corrugation. In the composite corrugation Eq. (3), $\cos(n\gamma x)$ describes the high frequency composition and $\sin(\gamma x)$ does the low frequency one. The position vector of a point on \mathcal{S} can be then described by $\mathbf{r} = x\mathbf{e}_x + y\mathbf{e}_y + a \cos(n\gamma x) \sin(\gamma x)\mathbf{e}_z$,

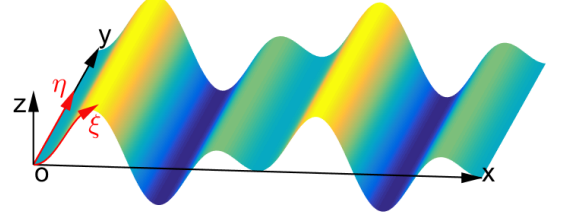


FIG. 1. (Color online) Schematic of a surface reconstructed by a dual-frequency corrugation given by $z = a \cos(n\gamma x) \sin(\gamma x)$. Here a and $2\pi/\gamma$ are the amplitude and period length of corrugation, respectively. n is a nonzero positive integer. (ξ, η) denotes the two curvilinear coordinate variables over surface.

and hence that of a point in the immediate region near to \mathcal{S} can be parameterized by $\mathbf{R} = \mathbf{r} + q_3\mathbf{e}_n$, \mathbf{e}_n is the unit vector basis normal to \mathcal{S} , and q_3 is the corresponding coordinate variable. According to the definitions $G_{ij} = \partial_i \mathbf{R} \cdot \partial_j \mathbf{R}$ and $g_{ab} = \partial_a \mathbf{r} \cdot \partial_b \mathbf{r}$, wherein $(i, j = 1, 2, 3)$ and $(a, b = 1, 2)$, we obtain

$$g_{ab} = \begin{pmatrix} 1 & 0 \\ 0 & 1 \end{pmatrix} \quad (4)$$

and

$$G_{ij} = \begin{pmatrix} f^2 & 0 & 0 \\ 0 & 1 & 0 \\ 0 & 0 & 1 \end{pmatrix}, \quad (5)$$

respectively. It is easy to check the relationship between G and g , $G = f^2 g$, where the rescaling factor f is

$$f = 1 + \frac{a[(1+n^2)\cos n\gamma x \sin \gamma x + 2n \cos \gamma x \sin n\gamma x]}{[1 + a^2(\cos \gamma x \cos n\gamma x - n \sin \gamma x \sin n\gamma x)^2]^{3/2}} q_3. \quad (6)$$

In terms of the above discussions, by using the formula of the geometric influence^{14,26,27}, the effective Hamiltonian can be calculated as

$$\mathbf{H}_{\text{eff}} = \langle \chi_{0_n} | f^{\frac{1}{2}} \hat{\mathbf{H}} f^{-\frac{1}{2}} - \hat{\mathbf{H}}_n | \chi_{0_n} \rangle_0 = -\frac{\hbar^2}{2m^*}(\partial_\eta^2 + \partial_\xi^2) + V_g, \quad (7)$$

where $\hat{\mathbf{H}}$ is the original Hamiltonian describing a free particle in a 3D curvilinear coordinate system with $\hat{\mathbf{H}} =$

$-\frac{\hbar^2}{2m^*} \frac{1}{\sqrt{G}} \partial_i \sqrt{G} G^{ij} \partial_j$, \hat{H}_n denotes the normal component of \hat{H} with $\hat{H}_n = -\frac{\hbar^2}{2m^*} \frac{\partial^2}{\partial q_3^2}$, and V_g is the well-known geometric potential^{12,13} that reads

$$V_g = -\frac{\hbar^2}{2m^*} \frac{a^2 \gamma^4 [(1+n^2) \cos n\gamma x \sin \gamma x + 2n \cos \gamma x \sin n\gamma x]^2}{4[1 + a^2 \gamma^2 (\cos \gamma x \cos n\gamma x - n \sin \gamma x \sin n\gamma x)^2]^3}. \quad (8)$$

In the previous calculations, the wave function of the ground state $|\chi_{0c}\rangle$ is taken as the ground state of a harmonic oscillator with $w \rightarrow \infty$, that is

$$|\chi_{0n}\rangle = \alpha^{\frac{1}{2}} \pi^{-\frac{1}{4}} e^{-\frac{\alpha^2 q_3^2}{2}}, \quad (9)$$

where $\alpha = \sqrt{\frac{m w}{\hbar}}$. The evidence is that the geometric potential does not depend on the specific form of the confining potential and its relative strength^{28,29}. By virtue of the effective Hamiltonian Eq. (7), we directly write the effective Schrödinger equation as below

$$-\frac{\hbar^2}{2m^*} \left(\frac{\partial^2}{\partial \xi^2} + \frac{\partial^2}{\partial \eta^2} \right) \chi_s + V_g \chi_s = E_s \chi_s, \quad (10)$$

where η and ξ are two tangent coordinate variables of \mathcal{S} , respectively. Due to V_g only depending on x , and ξ just being a function of x , we can rewrite $\chi_s = \chi_\eta(\eta) \chi_\xi(\xi)$, and separate the effective quantum equation analytically into two components of η and ξ , they are

$$-\frac{\hbar^2}{2m^*} \frac{\partial^2}{\partial \xi^2} \chi_\xi + V_g \chi_\xi = E_\xi \chi_\xi \quad (11)$$

and

$$-\frac{\hbar^2}{2m^*} \frac{\partial^2}{\partial \eta^2} \chi_\eta = E_\eta \chi_\eta,$$

respectively, where $E_s = E_\xi + E_\eta$.

It is worthwhile to notice that in the original Schrödinger equation Eq. (2) the metric tensor G_{ij} depends on q_3 , while in the effective Schrödinger equation the metric g_{ab} does not. In the thin-layer quantization procedure, the original q_3 dependence of the metric G_{ij} changes into a geometric potential to keep the consistency of the effective Schrödinger equation. As a central result of contributions of the thin-layer quantization scheme, the geometric potential is presented in the effective Hamiltonian and plays an important role in the effective dynamics. The geometric potential is induced by curvature, therefore it can be reconstructed by designing the geometry of the investigated system. In the present model, the most difference in corrugation is that it is composed by dual frequencies compared to the usual single-frequency corrugation.

To learn the actions of composite corrugation on the geometric potential, the geometric potential is pictured in Fig. 2 as a function of γx and a with $m^* = 0.067m_0$, m_0 is the static mass of electron. In this case, the substrate of the composite corrugation is GaAs. Obviously, the result shown in Fig.(a) is in nice agreement with that given

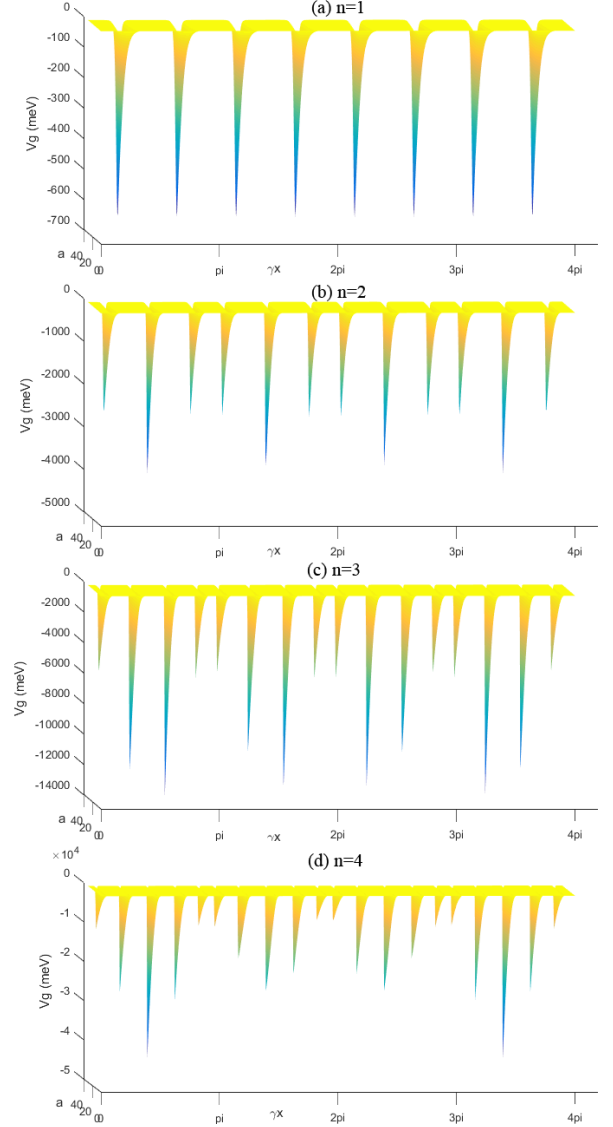


FIG. 2. (Color online) Surfaces of V_g as function of γx and a , a ranging from 0 to $30nm$ and γx varying in the region $[0, 8\pi]$, for (a) $n = 1$, (b) $n = 2$, (c) $n = 3$ and (d) $n = 4$.

by our another paper⁵. When the multiple frequency number n has a large integer, such as $n = 2, 3, 4$, the identical attractive wells of Dirac combs have separated into many grades, i.e. the attractive wells have different depths (see Fig. 2 (b), (c) and (d)). It is worthwhile to notice that the grade number is closely related to the multiple frequency number, and the shallowest wells in the case of n with a large integer are still deeper than

those with a small integer. It is shown that the corrugation can substantially affect the geometric potential. As a consequence, we can construct particular Dirac combs³⁰ by introducing a composite corrugation, tuning its amplitude a , and adjusting the multiple frequency number n .

III. TRANSMISSION PROBABILITY AFFECTED BY A COMPOSITE CORRUGATION

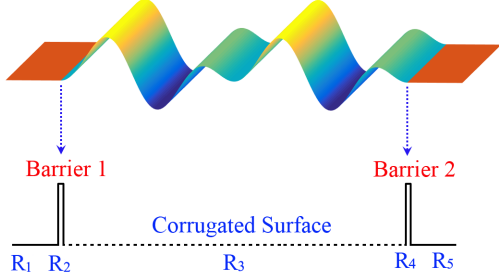


FIG. 3. (Color online) Schematic of the simplified model. R_1 and R_5 correspond to two leads, R_2 and R_4 describes the two potential barriers resulting from the boundaries between adjacent regions in which an electron has different effective masses, R_3 is a surface reconstructed by a composite corrugation.

From Eq. (11) and the compositely corrugated surface \mathcal{S} Eq. (3), the effective Schrödinger equation can be re-expressed in x as

$$-\frac{\hbar^2}{2m^*} \frac{1}{\Delta} \frac{d}{dx} \left[\frac{1}{\Delta} \frac{d}{dx} \psi(x) \right] + V(x) \psi(x) = E \psi(x), \quad (12)$$

where $m^* = 0.067m_0$, m_0 is the static mass of an electron, if $x \in R_3$ and $m^* = m_0$ otherwise,

$$\Delta = \sqrt{1 + a^2 \gamma^2 (\cos n\gamma x \cos \gamma x - n \sin n\gamma x \sin \gamma x)^2}$$

if $x \in R_3$ and $\Delta = 1$ otherwise, ψ is a wave function, E is the energy with respect to ψ , and $V(x)$ stands for the potential of the simplified model (see Fig.3), that is

$$V(x) = \begin{cases} 20meV, & x \in R_2, \\ V_g(x), & x \in R_3, \\ 20meV, & x \in R_4. \end{cases} \quad (13)$$

The potential mainly includes three parts, two barriers and a geometric potential region. In the rest two parts R_1 and R_5 , the potential vanishes. Here $V_g(x)$ stands for the geometric potential (8) and meV denotes milli electron volts.

To study the action of the composite corrugation on the electronic transport, in what follows we will study the transmission probability of electron in the model Fig.3 by the transfer matrix technique³¹. In the discussed models

including a single-frequency corrugation^{5,32}, the boundaries constructed by two different materials, in which electrons have different effective masses, create resonant tunneling peaks and valleys. These results are still valid to the case of including composite corrugation. Although the model including a single-frequency corrugation has been discussed widely^{5,33,34}, the case of composite corrugations (see Fig. 3) is still rarely discussed. Now we pay all our attentions on the effects of composite corrugation on the transmission probability. We consider a model which consists of two barriers and a thin film with composite corrugation.

In the case of including a surface reconstructed by a dual-frequency corrugation, the corresponding geometric potential V_g can be exactly determined as Eq. (8). And we can then calculate the transmission probability by using the transfer matrix method with $m^* = 0.067m_0$ in R_3 and otherwise $m^* = m_0$. Subsequently, the transmission probability as a function of the incident energy E and the amplitude a of the composite corrugation is described in Fig. 4 for (a) $n = 1$, (b) $n = 2$, (c) $n = 3$ and (d) $n = 4$, respectively. It is straightforward to see that there are resonant tunneling peaks and valleys of transmission probability, which are mainly created by the boundaries constructed by two different materials. This result is in full agreement with that in Ref.⁵. In striking contrast to the known results, there is a fascinating result, the transmission gaps become wider and tunneling peaks become sharper. The manifest phenomena is entirely determined by the composite corrugation, because that the composite corrugation generates a geometric potential which consists of attractive wells with different depths. And the attractive wells with different depths constitute different Dirac combs, which can reject electrons with particular incident energies. The reason is that electrons are scattered by those attractive wells. In the present model, the composite corrugation provides many Dirac combs with different attractive wells. As a consequence, the transmission gaps are extremely broadened. In other words, these interesting results are essentially from the geometry of composite corrugation introduced in R_3 of the present model. The multiple frequency number n is larger, the transmission gaps are wider and the resonant tunneling bands are sharper.

Mathematically, the transport distance is a function of the multiple frequency number n and the amplitude a of composite corrugation which can be expressed by

$$\xi = \int_{R_3} \sqrt{1 + a^2 \gamma^2 (\cos n\gamma x \cos \gamma x - n \sin n\gamma x \sin \gamma x)^2} dx.$$

According to the integral, the distance between adjacent wells obviously grows with increasing the corrugation amplitude, while the distance is affected by the growing of multiple frequency number n not obvious. Despite this, the transmission gaps are still widened by growing the positive integer value of n with a fixed a , the tunneling domains are narrowed and sharpened correspondingly (see Fig. 5). The reason is that n has larger value, the

number of attractive wells is more, the reflections correspondingly become stronger, that is the probability of electron reflected sharply growing. It is striking that the transmission gaps and tunneling domains are mainly contributed by the composite corrugation. As a potential

application, we can use composite corrugation to design an electronic switch, the transmission gaps mean that electron is reflected, but the tunneling domains do that electron can pass.

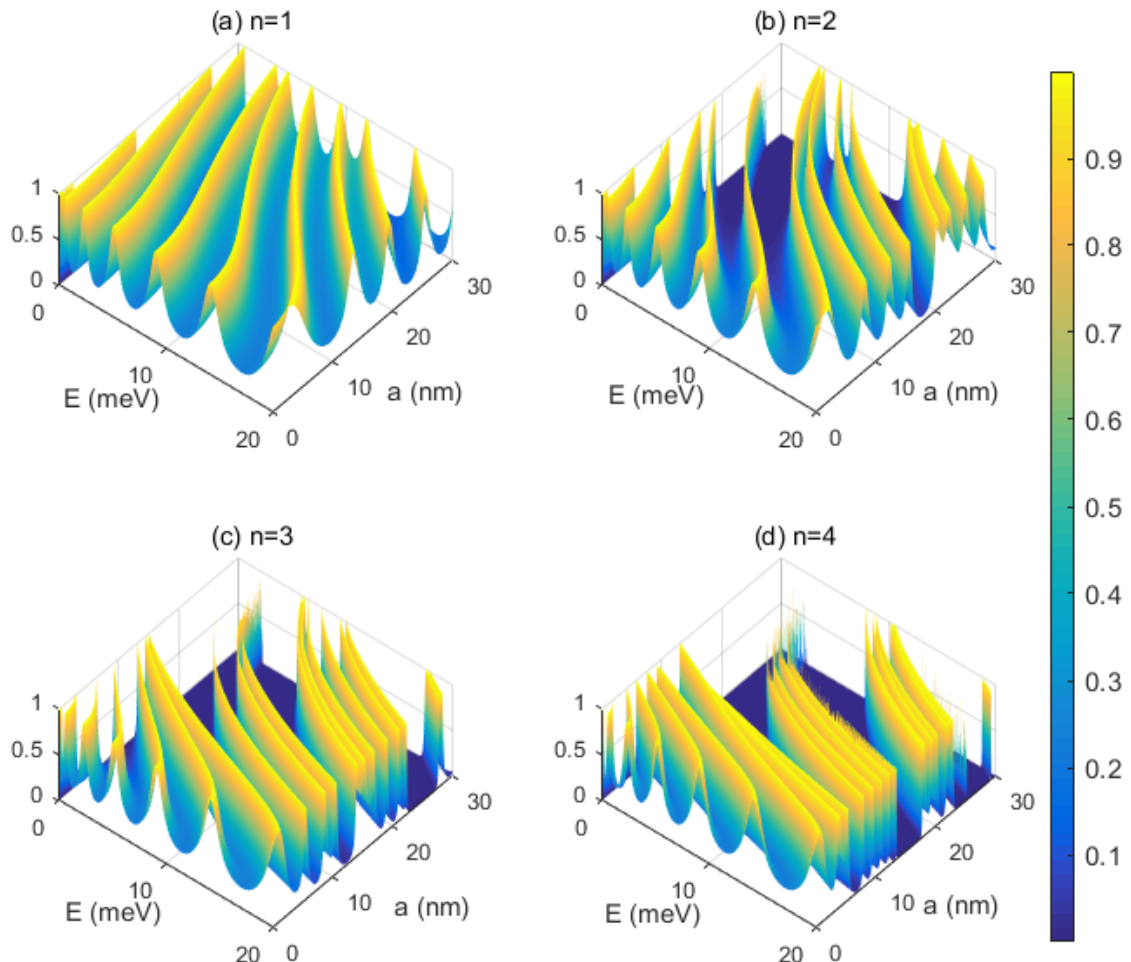


FIG. 4. (Color online) Transmission probability versus incident energy E and the amplitude a with $V(x) = 20\text{meV}$ in R_2 and R_4 , $V(x) = 0\text{meV}$ otherwise, $m^* = 0.067m_0$ in R_3 and $m^* = m_0$ otherwise, for (a) $n = 1$, (b) $n = 2$, (c) $n = 3$ and (d) $n = 4$.

IV. CONCLUSIONS

In the present paper, we have considered a 2D thin film including a particular part that is a surface reconstructed by a dual-frequency corrugation. The composite corrugation generates a geometric potential, which consists of many attractive wells with different depths, like Dirac combs. Due to the presence of two frequencies, the attractive wells have not identical depths. The diver-

sity of the well depth depends entirely on the multiple frequency number n . In other words, the presence of composite corrugation imposes many Dirac combs with different depth wells to scatter the electrons passing the compositely corrugated film. The depth of wells grows with increasing the amplitude a of the corrugation, and extremely increases with larger the multiple frequency number n . Approximately, these attractive wells can be roughly replaced by square wells. The square wells with

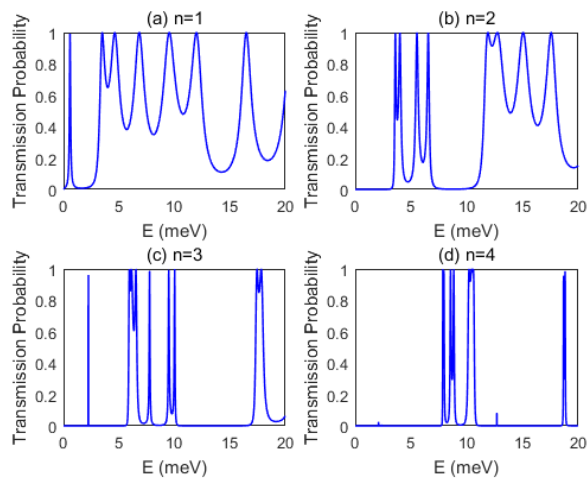


FIG. 5. (Color online) Transmission probability versus incident energy E with $a = 30nm$ and $m^* = 0.067m_0$ in R_3 , $m^* = m_0$ otherwise, for (a) $n = 1$, (b) $n = 2$, (c) $n = 3$ and (d) $n = 4$.

different depths can be structured by introducing periodically magnetic fields with different strengthes. By

using magnetic field determined by magnetic vector potential, the filter designed for electron with certain energy is named the vector-tunable filter³⁵. By designing the composite corrugation of film, the filter fabricated for electron with certain energy can be named as a geometry-tunable filter. In comparison to the single frequency corrugation, the composite corrugation provides more accesses to adjust the particular electron filter. As a particular application, the composite corrugation can be used to design curvature-tunable electronic switch when the multiple frequency number n is large enough.

ACKNOWLEDGMENTS

This work is jointly supported by the Natural Science Foundation of Shandong Province of China (Grant No. ZR2017MA010), the National Major state Basic Research and Development of China (Grant No. 2016YFE0129300), the National Nature Science Foundation of China (Grants No. 11690030, No. 11475085, No. 11535005, No. 61425018).

* wangonglong@lyu.edu.cn

† zonghs@nju.edu.cn

¹ S. Ono and H. Shima, *Phys. Rev. B* **79**, 235407 (2009).

² C. Ortix, S. Kiravittaya, O. G. Schmidt, and J. van den Brink, *Phys. Rev. B* **84**, 045438 (2011).

³ T. Kosugi, *J. Phys. Soc. Japan* **80**, 073602 (2011).

⁴ Y. Zhang, Z. Yan, K. Nan, D. Xiao, Y. Liu, H. Luan, H. Fu, X. Wang, Q. Yang, J. Wang, W. Ren, H. Si, F. Liu, L. Yang, H. Li, J. Wang, X. Guo, H. Luo, L. Wang, Y. Huang, and J. A. Rogers, *Proc. Nat. Acad. Sci.* **112**, 11757 (2015).

⁵ Y.-L. Wang, G.-H. Liang, H. Jiang, W.-T. Lu, and H.-S. Zong, *J. Phys. D: Appl. Phys.* **49**, 295103 (2016).

⁶ S. Gupta and A. Saxena, *J. Appl. Phys.* **109**, 074316 (2011).

⁷ J. Goldstone and R. L. Jaffe, *Phys. Rev. B* **45**, 14100 (1992).

⁸ H. Shima, M. Sato, K. Iiboshi, S. Ghosh, and M. Arroyo, *Phys. Rev. B* **82**, 085401 (2010).

⁹ B. Novakovic, R. Akis, and I. Knezevic, *Phys. Rev. B* **84**, 195419 (2011).

¹⁰ R. Cheng, Y.-L. Wang, W.-R. Cao, X.-J. Liu, and H.-S. Zong, *arXiv:1810.02098*.

¹¹ P. Schuster and R. Jaffe, *Ann. Phys.* **307**, 132 (2003).

¹² H. Jensen and H. Koppe, *Ann. Phys.* **63**, 586 (1971).

¹³ R. C. T. da Costa, *Phys. Rev. A* **23**, 1982 (1981).

¹⁴ Y.-L. Wang, H. Jiang, and H.-S. Zong, *Phys. Rev. A* **96**, 022116 (2017).

¹⁵ A. Szameit, F. Dreisow, M. Heinrich, R. Keil, S. Nolte, A. Tünnermann, and S. Longhi, *Phys. Rev. Lett.* **104**, 150403 (2010).

¹⁶ Q. H. Liu, C. L. Tong, and M. M. Lai, *J. Phys. A: Math. Theor.* **40**, 4161 (2007).

¹⁷ Q. H. Liu, L. H. Tang, and D. M. Xun, *Phys. Rev. A* **84**, 042101 (2011).

¹⁸ R. Spittel, P. Uebel, H. Bartelt, and M. A. Schmidt, *Opt. Express* **23**, 12174 (2015).

¹⁹ Y.-L. Wang, L. Du, C.-T. Xu, X.-J. Liu, and H.-S. Zong, *Phys. Rev. A* **90**, 042117 (2014).

²⁰ Y.-L. Wang and H.-S. Zong, *Ann. Phys.* **364**, 68 (2016).

²¹ M. Lohse, C. Schweizer, H. M. Price, O. Zilberberg, and I. Bloch, *Nature* **553**, 55 (2018).

²² M. Blencowe, *Phys. Rep.* **395**, 159 (2004).

²³ A. V. Chaplik and R. H. Blick, *New J. Phys.* **6**, 33 (2004).

²⁴ Z.-L. Xiang, S. Ashhab, J. Q. You, and F. Nori, *Rev. Mod. Phys.* **85**, 623 (2013).

²⁵ R. Amalraj and S. Sambandan, *J. Appl. Phys.* **116**, 164507 (2014).

²⁶ Y.-L. Wang, M.-Y. Lai, F. Wang, H.-S. Zong, and Y.-F. Chen, *Phys. Rev. A* **97**, 042108 (2018).

²⁷ Y.-L. Wang, M.-Y. Lai, F. Wang, H.-S. Zong, and Y.-F. Chen, *Phys. Rev. A* **97**, 069904 (2018).

²⁸ C. Ortix, *Phys. Rev. B* **91**, 245412 (2015).

²⁹ M. Encinosa, L. Mott, and B. Etemadi, *Phys. Scr.* **72**, 13 (2005).

³⁰ J. J. Sakurai and D. J. Kirkner, *Modern Quantum Mechanics* (Addison-Wesley, 1993).

³¹ Y. Ando and T. Itoh, *J. Appl. Phys.* **61**, 1497 (1987).

³² M. Encinosa, *IEEE Trans. Electron Devices* **47**, 878 (2000).

³³ H. Shima, H. Yoshioka, and J. Onoe, *Phys. Rev. B* **79**, 201401 (2009).

³⁴ S. Ono and H. Shima, *Phys. Rev. B* **79**, 235407 (2009).

³⁵ L. Dell'Anna and A. De Martino, *Phys. Rev. B* **80**, 155416 (2009).